Cemef

July, 9th 2018, Saint-Malo, France

Nucleated bubbles in glass former liquids undergoing coalescence and growth

D. Boloré (Surface du Verre et Interfaces, UMR 125 CNRS/Saint-Gobain) & F. Pigeonneau

Industrial Context

- Cullet is mainly used for the production of container glass:

Germany	88 %	Belgium	95 %	France	73 %
Poland	**43** %	Italy	76 %	Austria	93 %
United-Kingdom	64 %	Portugal	60 %	Spain	60 %
Sweden	**97** %	Holland	79 %	**Denmark**	**98** %

Table 1: Rates of glass recycling in Europe in 2013 [data SEVE].

- Advantages of introduction of cullet in raw materials:
  - Reductions of mineral resources;
  - Reduction of CO_2 release;
  - Reduction of the energy to provide.

Industrial Context

- Cullet is mainly used for the production of container glass:

Germany	88 %	Belgium	95 %	France	73 %
Poland	**43** %	Italy	76 %	Austria	93 %
United-Kingdom	64 %	Portugal	60 %	Spain	60 %
Sweden	**97** %	Holland	79 %	**Denmark**	**98** %

Table 1: Rates of glass recycling in Europe in 2013 [data SEVE].

- Advantages of introduction of cullet in raw materials:
  - Reductions of mineral resources;
  - Reduction of CO_2 release;
  - Reduction of the energy to provide.

What is the limitation to go forward 100 % of cullet?

1. Experimental set-up
2. Spatial distributions of nucleated bubbles
3. Bubble growth rate
4. Saturation and nucleation
5. Conclusion

1. Experimental set-up

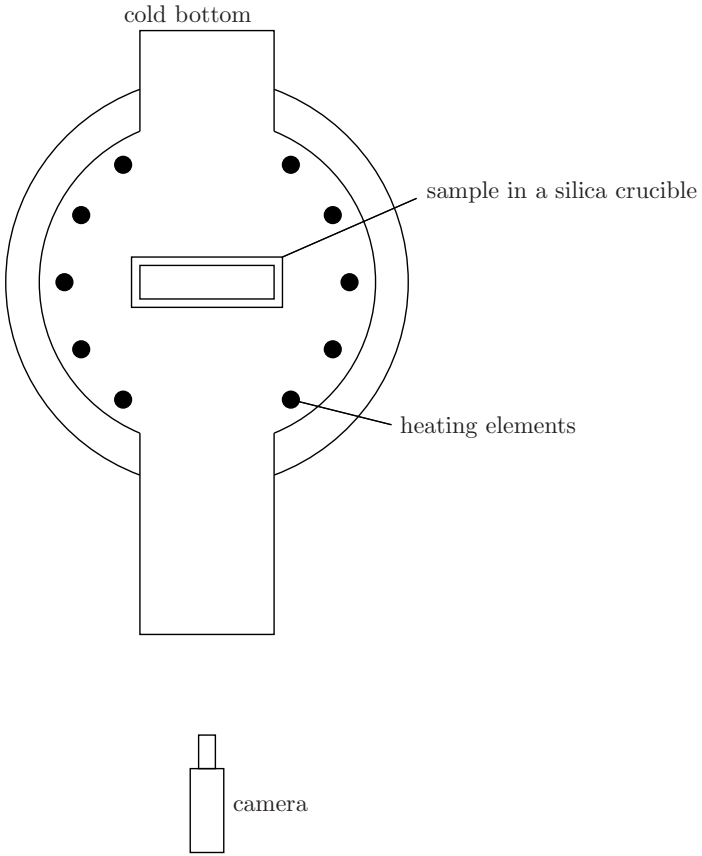

- Float glass samples are introduced in silica crucible;
- Recording of the melting and other events with 2 cameras (60 and 25 μm/px).

Figure 1: Sketch of HTO furnace.

SiO_2	Na_2O	CaO	MgO	Al_2O_3	SO_3	Fe_2O_3	FeO
72.4	13.85	8.88	3.74	0.73	0.22	0.055	0.014

Table 2: Composition of the glass samples (wt %).

2. Spatial distributions of nucleated bubbles

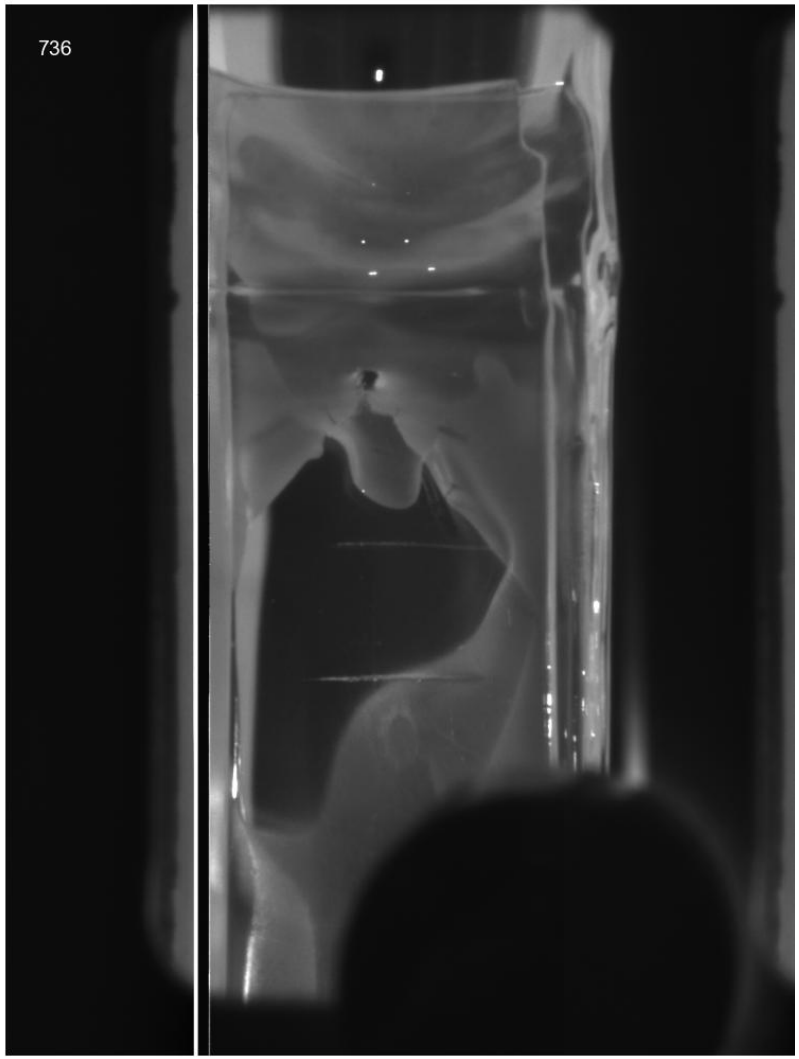

2. Spatial distributions of nucleated bubbles

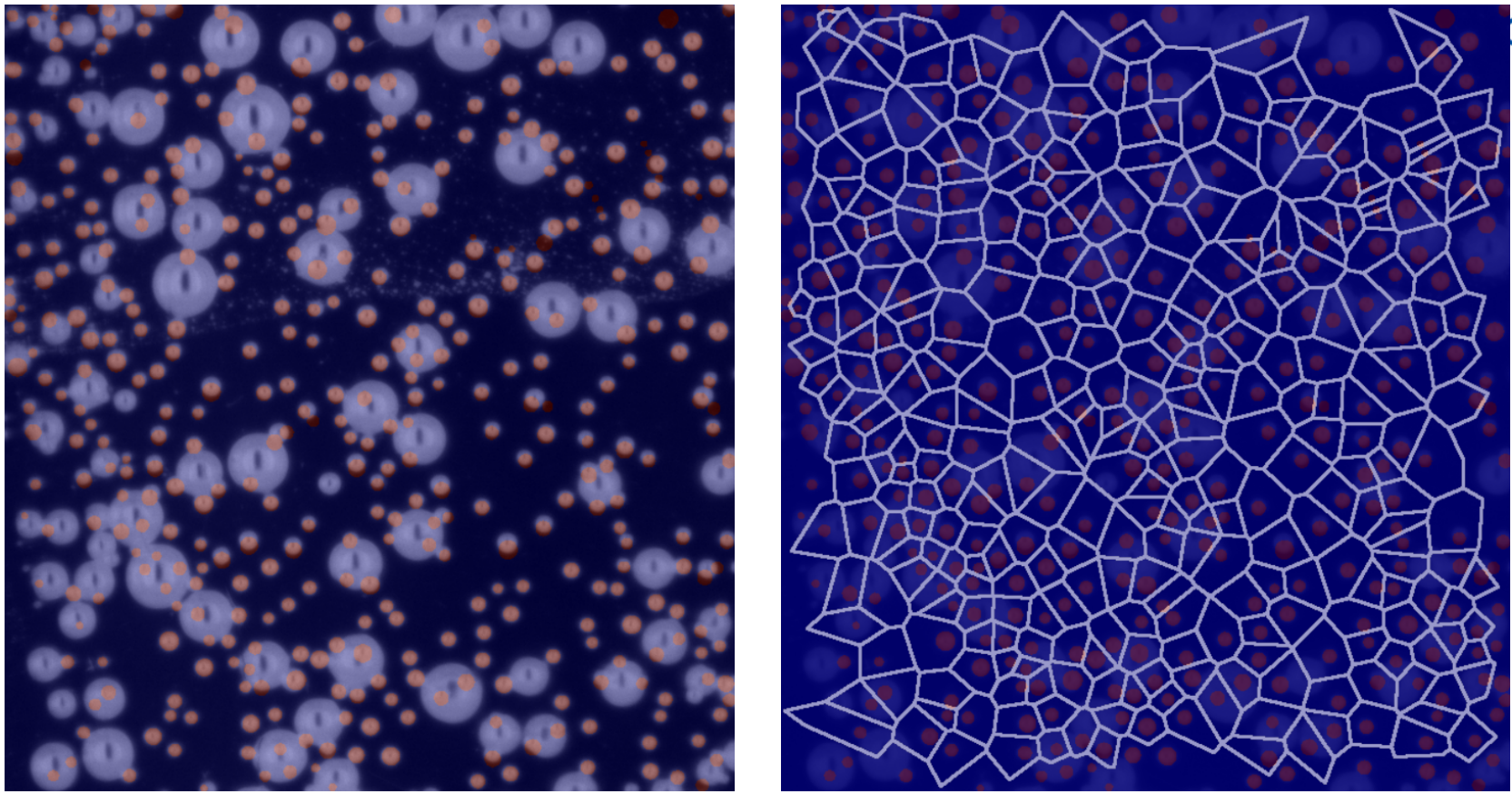

Figure 2: Detection of nucleation sites on each face of the crucible and Voronoï diagram of nucleation sites.

2. Spatial distributions of nucleated bubbles

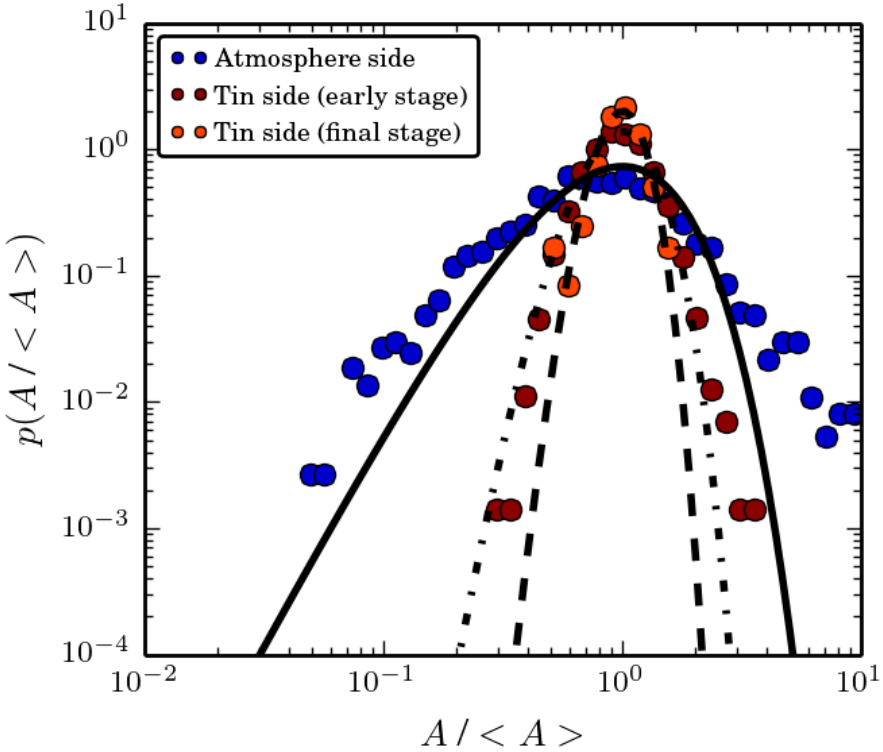

$$f(x) = n^n x^{n-1} e^{-nx}/\Gamma(n), \quad (1)$$

$$\text{with } x = \frac{A}{\langle A \rangle}.$$

- Atmosphere side: $n = 3.5$; Tin side: $n = 12.2$ at the beginning and $n = 25.5$ at the end.

Figure 3: PDF of the area of Voronoï cells.

- For objects randomly distributed over a surface, $n = 7/2$ [1].

[1] Ferenc, J.-S. & Néda, Z. (2007). *Physica A*, **385**:518–526

2. Spatial distributions of nucleated bubbles

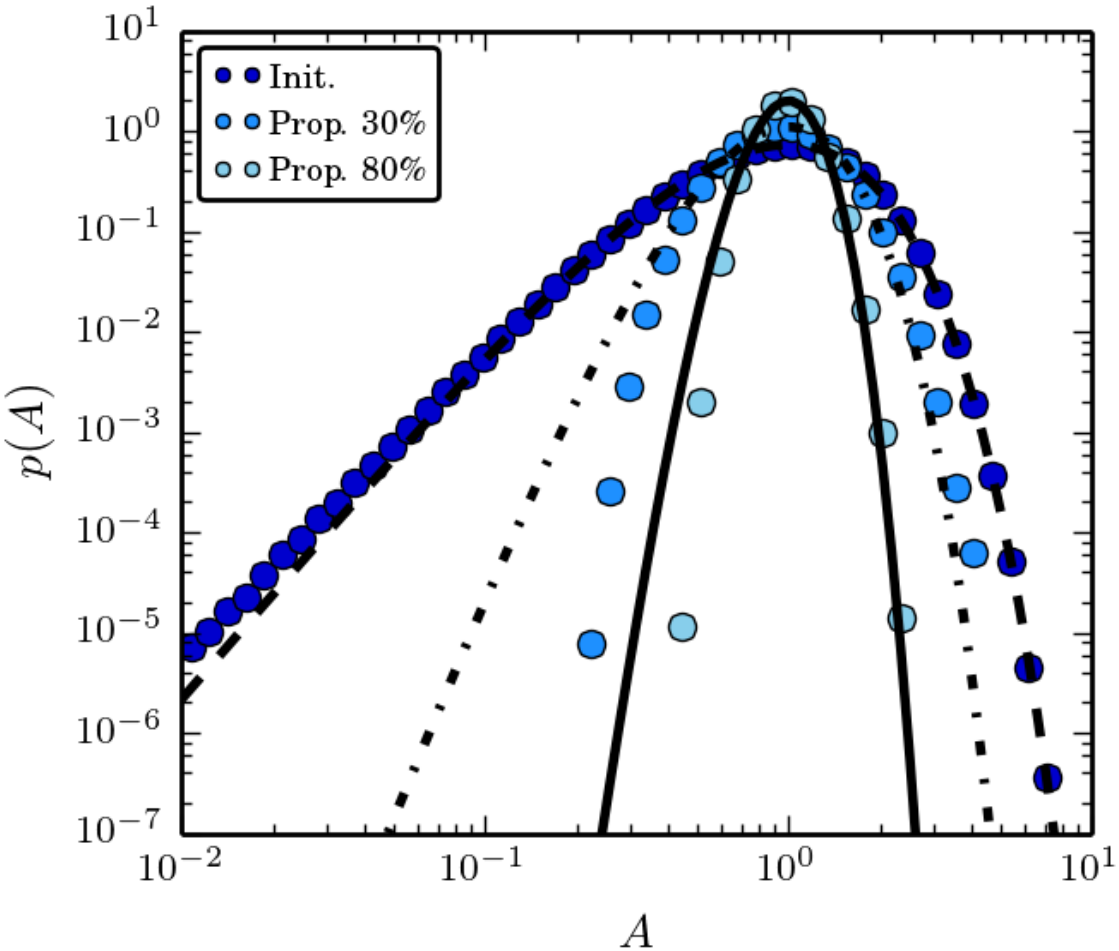

Figure 4: PDF of area of Voronoï cells obtained from the numerical simulations.

2. Spatial distributions of nucleated bubbles

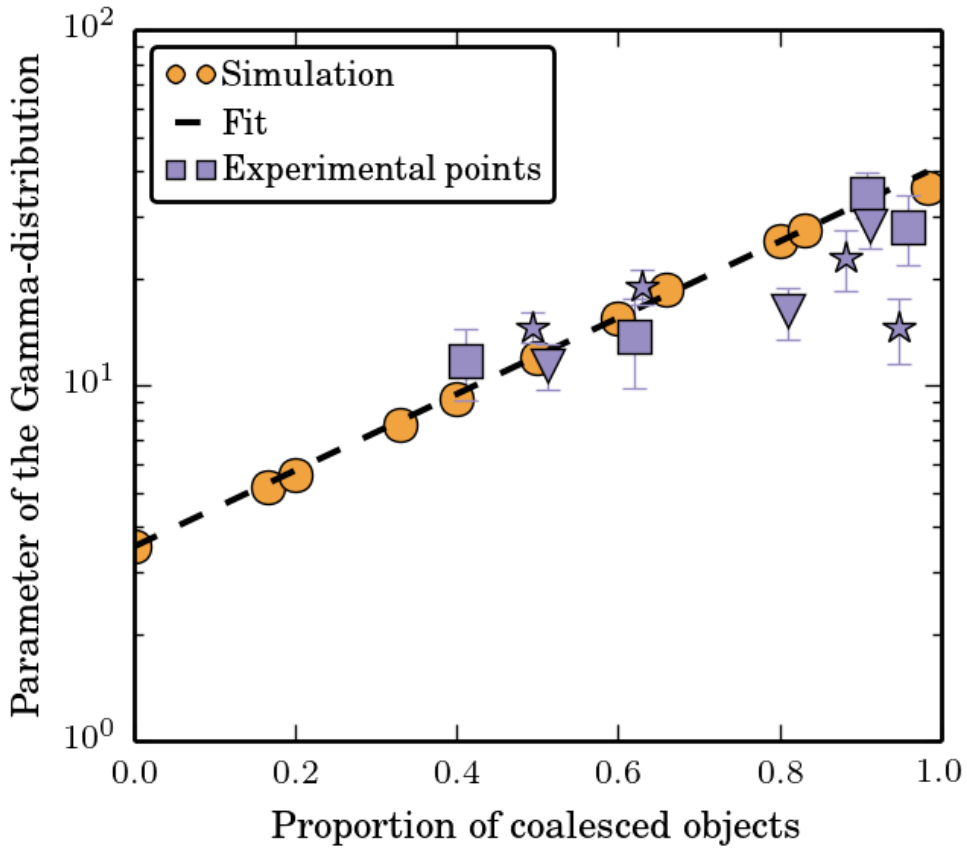

Figure 5: n vs. the proportion of coalesced objects.

$$n = \frac{7}{2} e^{2.47x}, \text{ with } x = \frac{d_0 - d}{d_0}. \tag{2}$$

2. Spatial distributions of nucleated bubbles

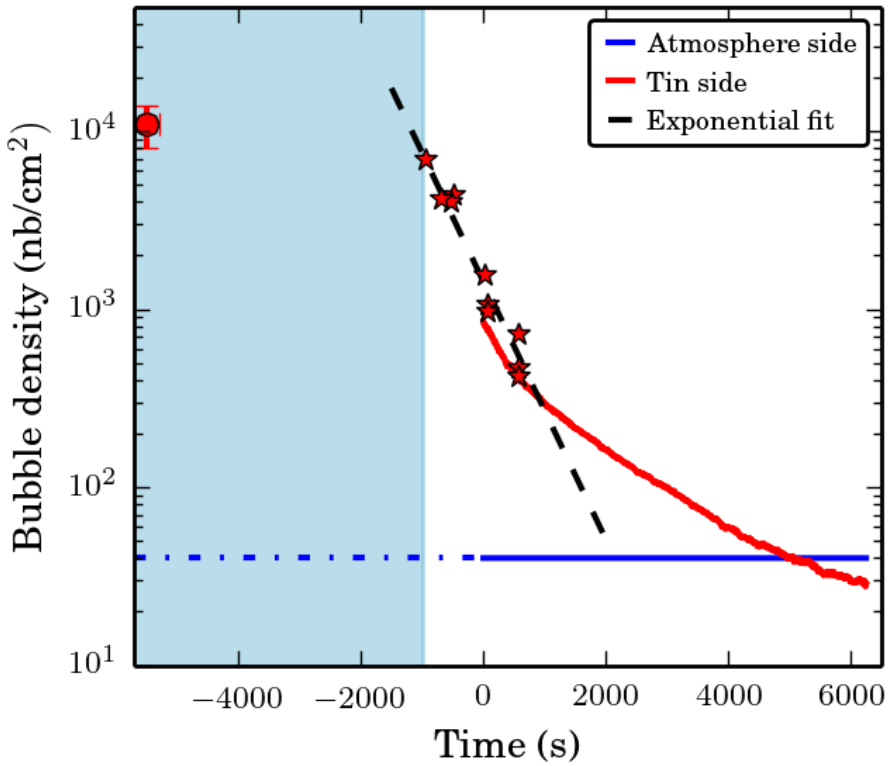

Figure 6: Bubble densities on the two sides of glass samples.

- In atmosphere side, $d_0 = 40$ nuclei/cm^2;
- In tin side, $d_0 = 9300$ nuclei/cm^2 (230 times larger).

3. Bubble growth rate

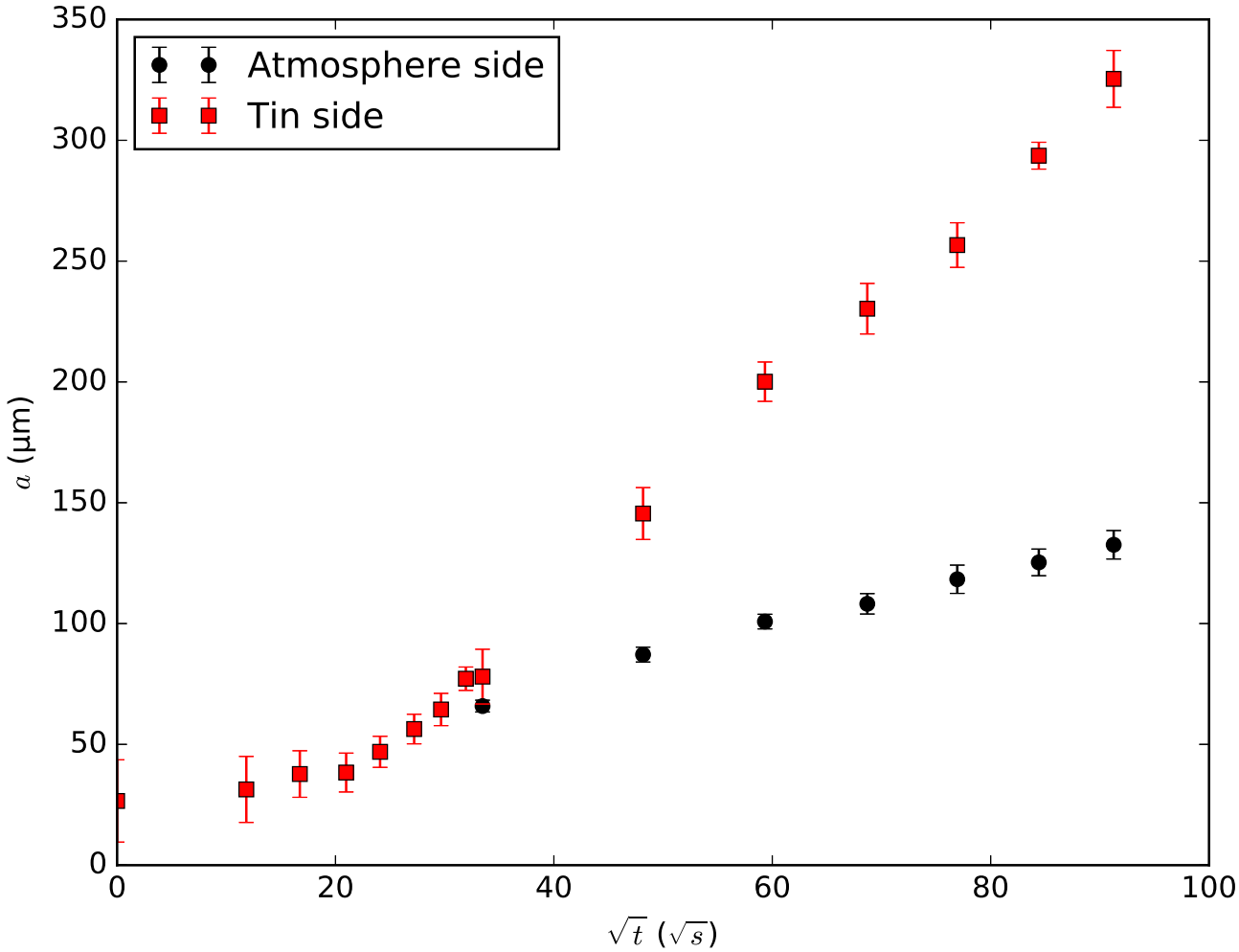

Figure 7: a (μm) vs. $\sqrt{t}$ ($\sqrt{\text{s}}$) for bubbles in tin and atmosphere sides of molten glass samples.

3. Bubble growth rate

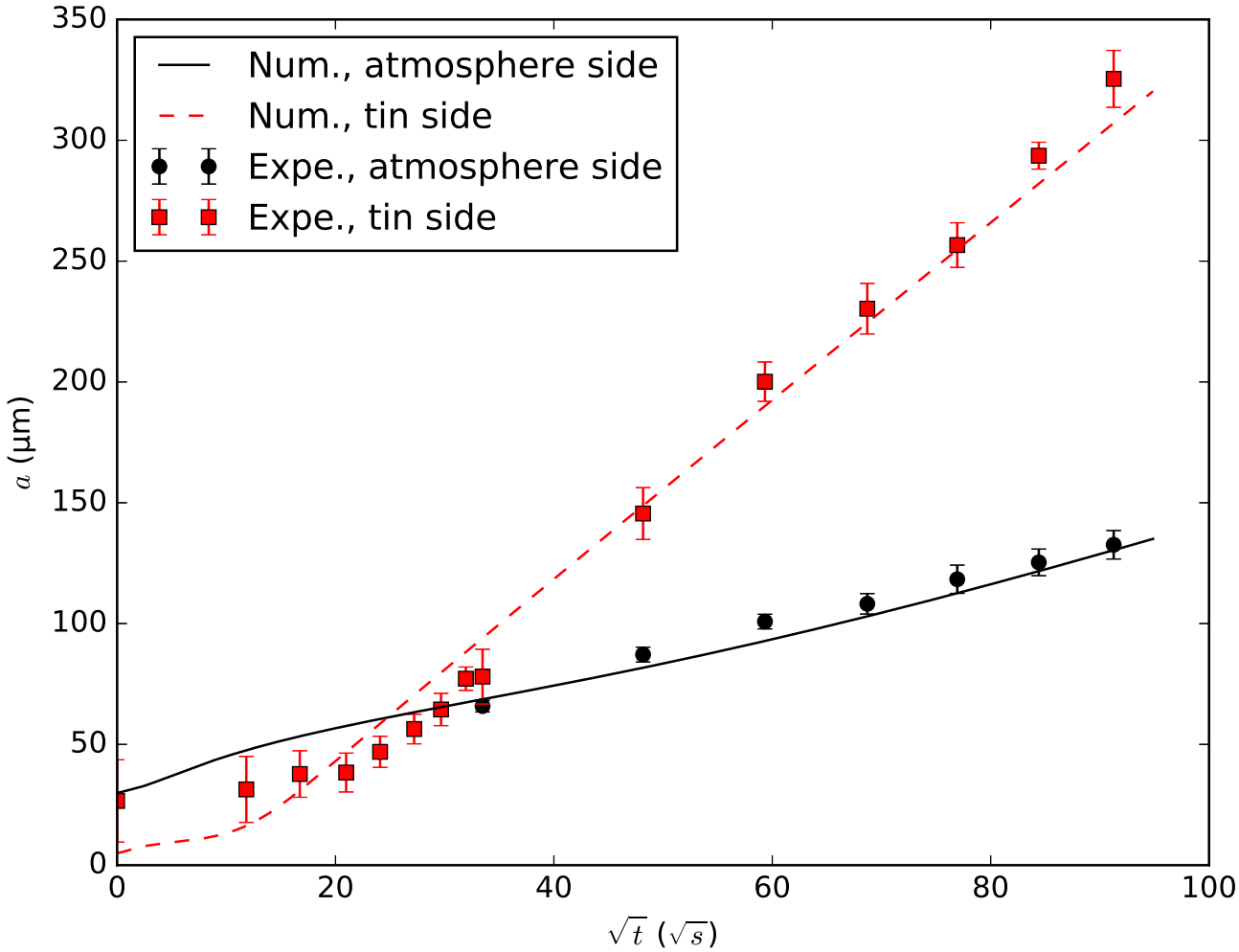

Figure 7: a (μm) vs. $\sqrt{t}$ ($\sqrt{\text{s}}$) for bubbles on tin and atmosphere sides of molten glass samples.

3. Bubble growth rate

- In the mass transfer modeling, we consider two redox couples[2]:

$$\mathrm{Fe}^{3+} + \frac{1}{2}\mathrm{O}^{2-} \rightleftharpoons \mathrm{Fe}^{2+} + \frac{1}{4}\mathrm{O}_2, \tag{3}$$

$$\mathrm{Sn}^{4+} + \mathrm{O}^{2-} \rightleftharpoons \mathrm{Sn}^{2+} + \frac{1}{2}\mathrm{O}_2. \tag{4}$$

- Using the experimental bubble growth rate, the "equilibrium" P_{O_2} is:
  - In atmosphere side, $P_{\mathrm{O}_2} = 1.3 \cdot 10^{-3}$ Pa;
  - In tin side, $P_{\mathrm{O}_2} = 4.1 \cdot 10^{-4}$ Pa.
- **Tin leads to a reduction of glass.**

[2] Pigeonneau, F. (2011). *Int. J. Heat Mass Transfer*, **54**:1448-1455.

4. Saturation and nucleation

- The critical bubble size for nucleation in the case of multi-species is given by

$$a_{\mathrm{cr}} = \frac{2\gamma}{\left(\sum_{i=1}^{N_g} Sa_{\mathrm{G}_i}^{1/\beta_{\mathrm{G}_i}} - 1\right) P_l}, \tag{5}$$

$$Sa_{\mathrm{G}_i} = \frac{C_{\mathrm{G}_i}}{L_{\mathrm{G}_i} P_l^{\beta_{\mathrm{G}_i}}}. \tag{6}$$

- The supersaturation for N_g dissolved species is

$$\sigma = \sum_{i=1}^{N_g} Sa_{\mathrm{G}_i}^{1/\beta_{\mathrm{G}_i}} - 1. \tag{7}$$

4. Saturation and nucleation

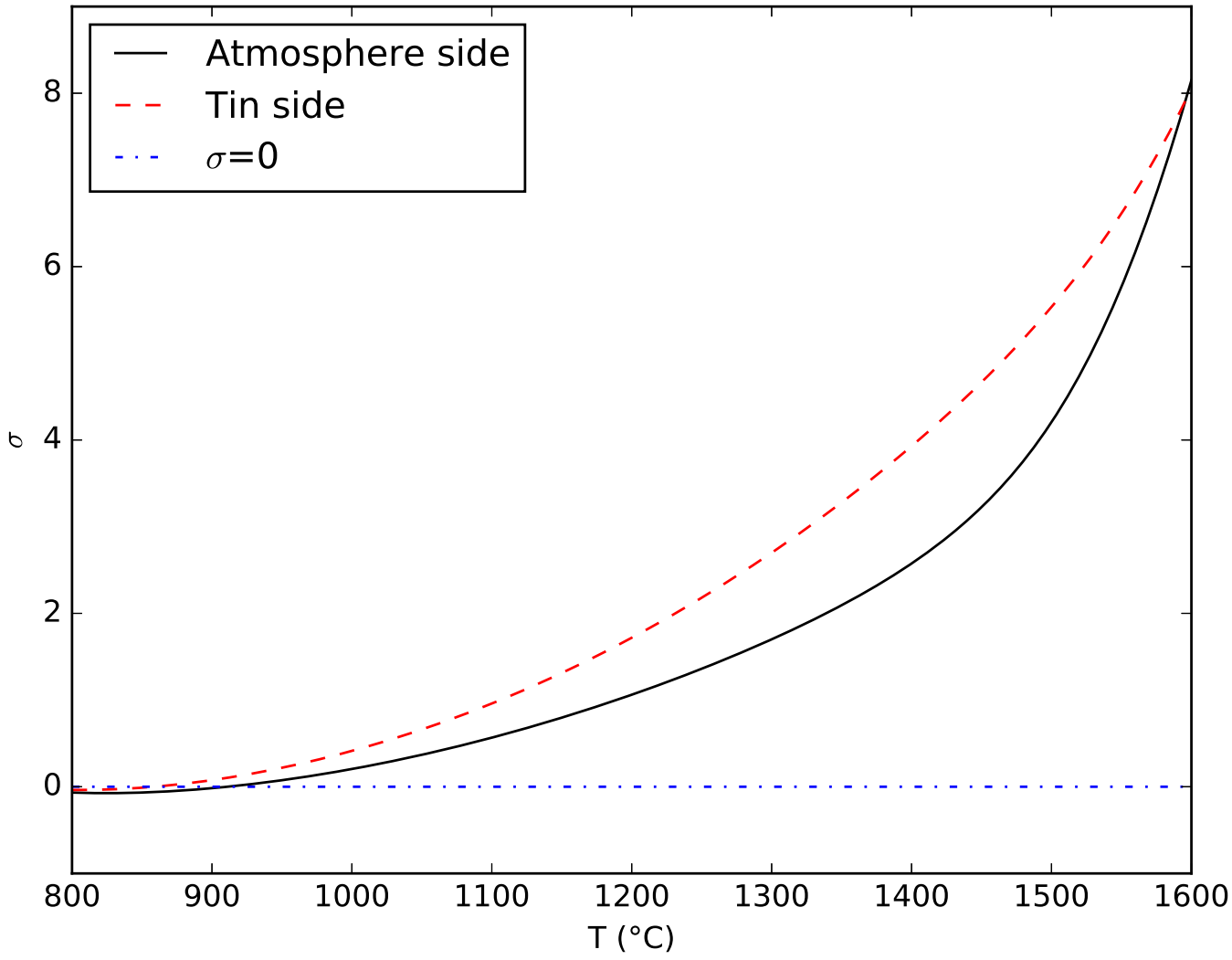

Figure 8: σ vs. T (°C) in atmosphere and tin sides.

5. Conclusion

- Remelting of cullet leads to a large bubble formation.
- Enhancements of the bubble nucleation and growth rate due to the tin pollution.
- The glass reduction on tin side is the main parameter controlling the bubble nucleation and the growth rate.
- Difficult to quantify the bubble nucleation rate (work in progress to improve the prediction).
- The 100 % of cullet is difficult to reach because the bubble creation persists and needs to introduce fining agents.
- See for more details[3].

[3] Boloré, D. & Pigeonneau, F. (2018). *J. Am. Ceram. Soc.*, **101**:1892-1905.